ACS APPLIED NANO MATERIALS

www.acsanm.org Article

Zr-Based Metal–Organic Framework Nanocrystals for Water Remediation

Asmaa Jrad,[⊥] Patrick Damacet,[⊥] Zahraa Yaghi, Mohammad Ahmad,* and Mohamad Hmadeh*

Cite This: *ACS Appl. Nano Mater.* 2022, 5, 10795–10808 Read Online

ACCESS | Metrics & More | Article Recommendations | Supporting Information

ABSTRACT: A series of derivatives of the Zr-based MOF UiO-66 were synthesized, fully characterized, and tested for their efficiency in the adsorption and removal of the highly toxic elements lead (Pb(II)), cadmium (Cd(II)), arsenate As(V), and selenite Se(IV). Different structural engineering techniques were employed to alter the properties of the Zr-MOFs, such as linker functionalization and defect creation to increase the density of adsorption sites. The functionalization of the UiO-66-based structures with carboxylate groups increased the removal efficiency of Pb(II) cations by more than 70% and that of Cd(II) cations by more than 60% to reach 125.2 and 69.1 mg/g, respectively. Moreover, the induced cluster defects were found to be the preferred adsorption sites of the anion pollutants. The adsorption of As(V) and Se(IV) by the high-defect UiO-66-200FA was 132.5 and 30.8 mg/g, respectively, which was higher than that of the less defect UiO-66, while almost no adsorption was achieved by UiO-66$(COOH)_2$. Furthermore, a multivariate (MTV-MOF) approach was employed to investigate the effect of the functional groups on the diffusion of the adsorbates within the porous networks. Interestingly, adsorption equilibrium was reached within minutes for the best-performing MOFs, highlighting their potential to be used in practical water treatment applications. Finally, chemical adsorption seemed to be dominant among binding mechanisms for all the pollutants, which were analyzed in detail to determine the characteristics that govern the adsorption efficiency of UiO-66-based adsorbents. The conclusions provided by this comprehensive study help serve as a guideline for future researchers aiming to employ UiO-66-based adsorbents by providing them with a deep understanding of the design strategies required to maximize the performance of this robust MOF.

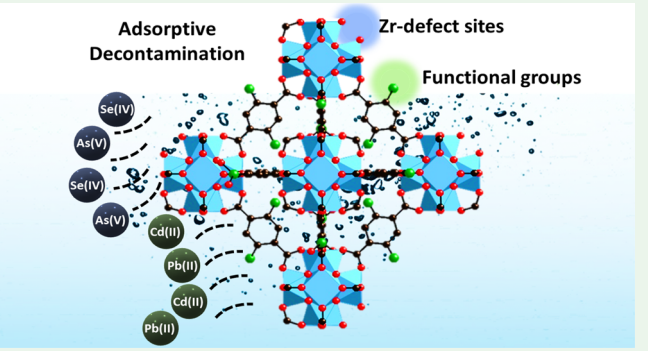

KEYWORDS: *Zr-MOFs, water treatment, structural defects, MTV-MOFs, heavy metal ions, chemical contaminants*

Downloaded via AMERICAN UNIV OF BEIRUT on August 6, 2024 at 11:08:19 (UTC).
See https://pubs.acs.org/sharingguidelines for options on how to legitimately share published articles.

INTRODUCTION

Water contamination is a global environmental concern that has attracted significant attention in the research field.[1] Chemical contaminants can reach water through different sources, which can be classified into two, (i) anthropogenic sources, such as industrial activities, runoff from agricultural lands, sewage systems, railways, landfills, and urban areas, which could contaminate groundwater reservoirs,[2] and (ii) natural or geological sources such as rocks, soil, and surface water, which can store, transport, and redistribute chemical contaminants.[3,4] Depending on the type of the pollutants and the significance of the exposure to them,[5] chemical contaminants can lead to detrimental health problems and are mostly toxic and carcinogenic.[6] Subsequently, many methods have been developed to remove these pollutants from water in the last two decades such as coagulation and flocculation, chemical precipitation, flotation, membrane filtration, ion exchange, electrochemical treatment technologies, electrodialysis, and adsorption.[7,8] Moreover, adsorptive water decontamination has been among the most famous methods in water treatment because of its high efficiency, lower cost, flexible design and operation, and the possibility that it offers to recycle and reuse adsorbents.[9]

Many adsorbents have been applied in water decontamination of heavy metal ions such as activated carbon, carbon nanotubes, zeolites, metal oxides, and others.[10−12] While part of these materials showed poor adsorption efficiency, selectivity, and recyclability,[10] other materials have been extensively used for their potential in the field such as nanosized metal oxides (NMOs) and zeolites. However, although NMOs are known for their large surface area and superior activity, they suffer from stability issues which cause them to aggregate and lose their efficiency with time.[13] Moreover, while zeolites are efficient

Received: May 14, 2022
Accepted: July 12, 2022
Published: July 26, 2022

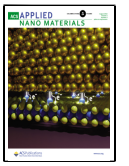

ACS Publications

© 2022 The Authors. Published by American Chemical Society

Scheme 1. Schematic Illustration of the Synthesis Details of the Nine Tested MOF Adsorbents[a]

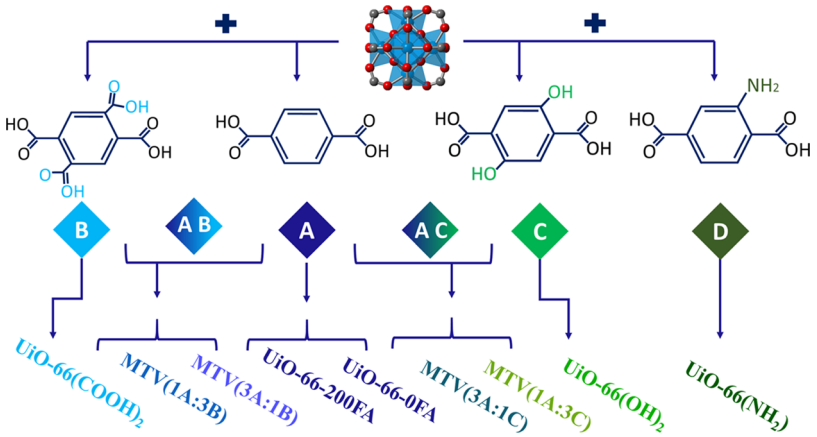

[a]The ratios indicated for MTV samples are molar ratios used in the synthesis mixture.

adsorbents with excellent ion exchange capabilities, chemical stability, and uniform pores,[14] the control of their crystalline structure, chemistry, porous network, and surface area using a predetermined design strategy for a specific application remains a challenge.[15] Consequently, the field is now in great need of novel adsorbents with excellent adsorption capacity and selectivity, high stability, ease of recyclability, and the flexibility to be designed and tuned for a specific application.

Metal−organic frameworks (MOFs) are a novel class of porous crystalline materials that have emerged in the last three decades and attracted a lot of attention in the adsorption field.[16] MOFs are composed of two main building blocks: (i) the metal cluster or the secondary building unit (SBU) and (ii) the organic linkers which connect the metal clusters to form 1D, 2D, or 3D periodic network structures.[17] Many characteristics make MOFs great candidates in the adsorption field such as their very large surface areas and their high and permanent porosities, which are essential for the diffusion of contaminants into the porous network to reach their adsorption sites.[18] Additionally, MOFs could be very flexibly designed to tune their surface area, the form and size of their pores, and the type and density of their adsorption sites. This is possible through the rational choice of the organic linker and metal cluster, which not only controls the type of adsorption sites in the structure but their connectivity and porosity as well.[19] Additionally, other strategies could be adopted to further tune the characteristics of MOFs by altering the synthesis conditions or by following postsynthetic modifications (PSMs), which could also activate the cluster, functionalize the linker, or allow the use of the porous network as a host for active guest molecules.[20,21] The control of the density and type of adsorption sites is essential in the adsorption process, as it dictates the strength and type of interactions between the MOF structure and the contaminants, which determine the selectivity and capacity of adsorption.[22] These exceptional traits made MOFs popular in a very wide range of applications such as gas storage,[23,24] catalysis,[25,26] separation,[27,28] drug delivery,[29,30] sensing,[31,32] bioimaging,[33,34] and proton conduction.[35,36] The competitive performance of MOFs in a variety of applications has pushed the research in the field to look for strategies to use MOFs in conventional separation systems. Since MOFs are mostly synthesized in the powder form, many studies aimed to incorporate MOFs in matrices that make their use more practical as adsorbents for water treatment. An example would be the incorporation of MOFs in electrospun membranes by mixing them in the electrospinning polymeric solution and using the membrane for the adsorption/filtration of heavy metal ions.[37−39] Other methods include the immobilization of MOFs in cotton fabric for the removal of dyes and pesticides from water[40] or the incorporation of MOFs in porous cellulose acetate membranes for the removal of pharmaceutical residues[41] and pesticides[42] from water.

However, MOFs have relatively lower stability than that of other adsorbent counterparts, so it is essential that the structures selected as adsorbents be stable in water and at the pH required for the adsorption of these materials and the adsorption conditions. This is why the development of the Zr-based MOF UiO-66 has gained a lot of attention, as it shows superior chemical and thermal stability among MOFs, which expanded its range of applications.[43] UiO-66 is composed of hexa-nuclear Zr clusters that are connected with 12 terephthalate linkers that are behind its high chemical and thermal stability.[44,45] UiO-66 and its functionalized derivatives, such as UiO-66(NH_2), UiO-66(NO_2), and UiO-66($CCOH)_2$, have been previously used as adsorbents for the removal of heavy metals,[19,22,46−48] dyes,[49] fluoride,[50] diclofenac sodium,[51] and other water contaminants. The explored adsorption mechanism of pollutants on the UiO-66-based adsorbents often included acid−base interactions,[48,50,51] $\pi-\pi$ stacking interactions,[51] and electrostatic attraction.[49,52] Although some studies explored the potential of UiO-66 adsorbents in water decontamination from chemical pollutants by functionalizing the organic linker[46] or by defect engineering to boost the structure's acidic character,[48] these studies remain rare and do not include a wide range of chemical contaminants. Additionally, to the best of our knowledge, there are not any studies that combine modulation synthesis with linker functionalization to maximize the efficiency of the UiO-66-based adsorbents. Furthermore, the mixed-linker approach has also never been used to fine-tune the structures' functionality without compromising on the surface area and pore volumes' levels. Given the extreme flexibility in the design and tuning of the UiO-66 structure, more work is required to take advantage of the potential that this MOF has to offer in the adsorption field for water decontamination. In this study, we report the synthesis of nine different UiO-66-based MOFs that are used for the decontamination of water from the cationic and anionic toxic pollutants (e.g., Pb(II), Cd(II), As(V), and Se(IV)). This study will focus on the effect of (i) defects, by synthesizing high-defect structures using modulation synthesis, (ii) linker functionaliza-

https://doi.org/10.1021/acsanm.2c02128
ACS Appl. Nano Mater. 2022, 5, 10795−10808

tion, by including in addition to UiO-66, UiO-66(COOH)$_2$, UiO-66(OH)$_2$, and UiO-66(NH$_2$), and (iii) the effect of partially functionalizing the structure with acidic groups through the mixed-linker or multivariate (MTV) approach by changing the ratio of the functionalized linker to terephthalic acid. All synthesized MOFs are fully characterized and tested as adsorbents for all the previously mentioned pollutants. The characterization techniques used are powder x-ray diffraction (PXRD), scanning electron microscopy (SEM), thermogravimetric analysis (TGA), Brunauer−Emmett−Teller (BET) surface area analysis, and proton nuclear magnetic resonance (^{1}H-NMR). This allows obtaining a detailed description of the MOF morphology, crystal size, surface area, pore volume, defect number, and the percentage of incorporation of each linker in the MTV structures. The performance of the MOF adsorbents was compared in the adsorption of the different contaminants, and a kinetic study was performed for the best-performing MOFs. The study aims to understand the role of the different UiO-66-based adsorbents' components in the adsorption process to serve as a guide for future engineering of these robust materials in the adsorption field.

MATERIALS AND METHODS

Materials and General Synthesis Procedure. The chemicals that have been used for the synthesis, characterization, and testing of the MOF adsorbents in water decontamination were purchased commercially and directly used without additional purification. Details on the chemical reagents and the suppliers are provided in Section 1 of the Supporting Information.

In this study, nine different MOF adsorbents were synthesized using a solvothermal method where an equimolar mixture of the metal salt $ZrCl_4$ (1.48 mmol) and the corresponding organic linker (1.48 mmol) was dissolved in *N*,*N*-dimethylformamide (DMF, 517 mmol) with the adequate amount of a modulator by sonication for 10 min. They were then placed in a preheated oven at 120 °C for 21 h. MOF adsorbents were synthesized using 200 molar equivalents of formic acid (FA) with respect to $ZrCl_4$, except for UiO-66, which was synthesized both with (UiO-66-200FA) and without (UiO-66) a modulator (Scheme 1). Other MOFs synthesized were UiO-66(COOH)$_2$, UiO-66(OH)$_2$, UiO-66(NH$_2$), and mixed-linker MOFs or multivariate MOFs (MTV), which were MTV(3A:1B), MTV(1A:3B), MTV(3A:1C), and MTV-(1A:3C), where A, B, and C refer to the organic linkers used for the synthesis of UiO-66, UiO-66(COOH)$_2$, and UiO-66(OH)$_2$, respectively, while the numbers before the letters indicate the ratio of incorporation of the corresponding linker in the synthesis mixture. After 21 h in the oven, the obtained precipitate is separated from the liquid part by centrifugation and is washed three times using DMF and then three times using dichloromethane (DCM). Every wash takes at least 2 h. The washed MOF is then placed in a vacuum oven overnight for thermal activation at 170 °C. The obtained activated MOF is then used for full characterization and testing. Scheme 1 and Table S1 in the Supporting Information give more details on the synthesis procedure of all MOF adsorbents tested in this study.

Adsorbent Characterization. To gain a detailed description of the MOF adsorbents' properties, all synthesized samples were characterized following their activation. Powder X-ray diffraction patterns (PXRD) of the adsorbents were recorded using a Bruker D8 advance X-ray diffractometer with a Cu Kα radiation (k = 1.5418 Å), 40 kV voltage, and 40 mA current, while the 2θ range was between 4 and 50°, at an increment of 0.02° (Bruker AXS GmbH, Karlsruhe, Germany). The thermal stability and defect number of the synthesized adsorbents were assessed using thermogravimetric analysis (TGA), where a 5−10 mg sample is weighed using a microbalance and placed in a platinum crucible to undergo the analysis. The crucible is then placed in the autosampler Netzsch TG 209 F1 Libra TGA apparatus, which places the sample in an oven and heats it in the presence of air from 30 °C to 1100 °C at 10 K·min^{-1} heating rate. The crystal morphology and size were evaluated using scanning electron microscopy (SEM). For SEM imaging, a very small amount of the MOF is placed on a conductive carbon tape covering an aluminum SEM specimen stub, which is then coated with a thin layer of gold (around 25 nm) and placed in a MIRA3 Tescan electron microscope for imaging. N_2 sorption measurements were performed at 77 K for all samples to assess their surface area and pore volume using a Micrometrics Gemini VII 2390p surface area analyzer, and the samples were degassed under a nitrogen flow at 170 °C overnight before the analysis. The BET equation was fitted in a P/P_0 between 0.0725 and 0.9919, and the pore volume was measured at P/P_0 = 0.991. Proton nuclear magnetic resonance (^{1}H-NMR) spectra were acquired using a C500 Bruker spectrometer (^{1}H and ^{13}C NMR at 500 MHz) only for the MTV-MOFs to estimate the percentage of incorporation of the two linkers inside the framework. $NaHCO_3$ solution of 1 M in the D_2O solvent was used to dissolve 5 mg of each MTV-MOF in a ^{1}H-NMR tube. The chemical shifts are recorded in delta (δ) units expressed in ppm with respect to the internal standard tetramethylsilane (TMS). The Fourier transform infrared (FTIR) spectra were collected on a Thermo-Nicolet in the 600−2100 cm^{-1} range in the transmittance mode.

Adsorption Experiments. To investigate the adsorption process and removal of the four toxic contaminants from aqueous solutions by the different UiO-66-based adsorbents, several adsorption experiments were performed at room temperature. The effect of the initial concentration of the pollutants on the maximum uptake of the MOFs and the effect of the contact time between the MOFs and the pollutants on the adsorption efficiency were both studied. In short, the adsorption experiments were implemented by adding 5 mg of the adsorbents to 20 mL scintillation vials containing 10 mL of the adsorbate solutions with concentrations ranging from 10 to 600 ppm. These adsorbate solutions were prepared by dissolving the required amounts of lead nitrate, cadmium chloride anhydrous, sodium arsenate dibasic heptahydrate, and sodium selenite in water. The mixture of the solutions with known initial concentrations of contaminants and 5 mg of UiO-66-based adsorbents was placed on a Daihan ShkO-300 analog orbital shaker at room temperature. After 48 h, the solutions were centrifuged for 15 min to allow the MOF nanoparticles to settle at the bottom of Falcon tubes, and the supernatant was extracted by filtration. The concentration of the ionic contaminants remaining in the solution was then determined via atomic absorption spectroscopy (AAS). This allowed us to determine the equilibrium adsorption capacity, q_e (mg/g), i.e., the amount of the pollutant adsorbed (mg) per mass (g) of the adsorbate via eq 1

$$q_e = \frac{C_0 - C_e}{m} V \tag{1}$$

where C_0 and C_e (mg/mL) are the concentrations of the contaminants before and after the adsorption process, respectively, m (g) is the mass of the adsorbent used, and V (mL) is the total volume of the solution.

Following the initial screening process using all the UiO-66-based adsorbents, the best-performing structures were used for a detailed kinetic study using a similar procedure. Several solutions with different initial concentrations of the pollutants were prepared and placed on a shaker in the presence of 5 mg of the UiO-66-based adsorbents. A sufficient amount of the supernatants from the different mixtures was collected at different times and then analyzed via AAS to determine the remaining amount of Pb (II), Cd (II), Se (IV), and As (V). This allowed us to examine the uptake of different adsorbates as a function of the contact time with the best-performing MOF adsorbents.

Recycling of the MOF adsorbents. Desorption studies were performed to assess the stability, recyclability, and reusability of the best-performing MOF adsorbents. During each regeneration cycle, the post-adsorbing MOFs used for the adsorption of Pb (II) and Cd (II) were collected and treated with sodium nitrite for 18 h, whereas the MOFs used for the removal of As (V) and Se (IV) were recovered and soaked in methanol for 12 h to desorb contaminants. After the desorption process took place, the recycled MOFs were transferred into a thermostable OV-70 Daihan vacuum oven and dried out for 12 h at a temperature of 110 °C for the following adsorption cycle. This adsorption−desorption process was conducted and repeated four times

https://doi.org/10.1021/acsanm.2c02128
ACS Appl. Nano Mater. 2022, 5, 10795−10808

Table 1. Quantitative Results of the MOF Adsorbents' Characterization

MOF	functionalized linkers from ^{1}HNMR (%)	BET surface area (m^2/g)	pore volume (cm^3/g)	defect number from TGA	particle size from PXRD (nm)
UiO-66-0FA	0	1049	0.35	1.36	87
UiO-66-200FA	0	1812	0.73	1.87	331
UiO-66$(COOH)_2$	100	522	0.11	1.93	28
UiO-66$(OH)_2$	100	602	0.19	1.51	252
UiO-66(NH_2)	100	1723	0.63	2.02	172
MTV(3A:1B)	16	773	0.26	1.83	302
MTV(1A:3B)	61	609	0.16	1.98	38
MTV(3A:1C)	13	1290	0.46	1.33	45
MTV(1A:3C)	52	761	0.24	1.90	51

where AAS was utilized during each cycle to determine the adsorption capacities and regeneration percentages.

RESULTS AND DISCUSSION

MOF Characterization. *Powder X-Ray Diffraction.* The crystallinity and phase purity of the nine MOF adsorbents synthesized were confirmed by recording their PXRD patterns shown in Figure S1, which reveal sharp and narrow peaks in accordance with the simulated patterns of UiO-66. As for the mixed-linker structures, their PXRD patterns were compared to those of the single-linker structures for a narrow 2θ range, and the results are shown in Figure S2 in the Supporting Information. It could be noticed that there is a slight shift in the characteristic peaks to a lower 2θ range starting from the pure UiO-66 structure to the structures incorporating more functionalized linkers in the MTV-MOFs to the fully functionalized structures. This shift could be explained by a cell expansion caused by the increase in the incorporation of the functionalized linkers inside the structure, which is in accordance with Vegard's law.[53,54] The previous observation shows that there is homogeneous incorporation of the functionalized and BDC linkers in the MTV-MOFs and especially that no shoulder peaks could be noted in any of the MTV-MOF PXRD patterns, which would be the case if the synthesis yielded a physical mixture of two MOF structures rather than an MTV-MOF.[53] The average particle size of the different MOF adsorbents was assessed from the PXRD patterns using the Scherrer equation, and the results are shown in Table 1.

Proton Nuclear Magnetic Resonance (^{1}H-NMR). The percent incorporation of the functionalized linkers in the MTV-MOFs was either 25% or 75%, as is detailed in Table S1 in the Supporting Information. However, to estimate the actual percentage of incorporation of these functionalized linkers in the MTV-MOFs, a ^{1}H-NMR analysis was conducted, and the results are shown in Figures S3−S6 in the Supporting Information. The figures show that there are two singlets present in all spectra at the chemical shifts of δ = 7.85 ppm and δ = 8.43 ppm, which were attributed to the BDC linker and the remaining DMF inside the pores, respectively. The structures incorporating 1,2,4,5-benzenetetracaboxylic acid show an additional singlet at δ = 7.49, while those incorporating 2,5-dihydroxyterephthalic acid show a singlet at δ = 7.29 ppm. These additional singlets were attributed to the functionalized linkers being incorporated in the MTV structures, and the actual percent incorporation was calculated from the spectra, and the results are shown in Table 1. It could be seen that the addition of functionalized linkers in the synthesis mixture caused an increase in the actual percent incorporation in the final structure, as is also evident from the increase in the intensity of the singlets attributed to these linkers in the ^{1}H-NMR spectra. However, the BDC linkers' incorporation was slightly higher than its starting molar ratio for all MTV-MOFs synthesized.

Scanning Electron Microscopy (SEM). The morphology of the nine synthesized MOF adsorbents was assessed using SEM imaging, and the results are shown in Figure S7. UiO-66-200FA SEM images reveal the clear octahedron morphology of the crystals with a bigger particle size than that of other samples. Compared to UiO-66-0FA, the bigger crystal size could be attributed to the addition of 200 equiv of the formic acid modulator in the synthesis mixture of UiO-66-200FA, which competes with the BDC linker on the binding sites to the Zr cluster, which slows down the crystallization process, yielding bigger crystals. Additionally, the SEM images of UiO-66(NH_2) and MTV(3A:1B) also reveal a clear octahedral morphology, while UiO-66$(OH)_2$ crystals seem to have a truncated octahedron morphology. Other MTV-MOFs synthesized and UiO-66$(COOH)_2$ samples seem to have smaller intergrown crystals with a sphere-like shape. Since not all crystal sizes could be estimated through SEM given the very small particle size of some of the samples, PXRD patterns were used to assess the average particle size of the different MOF adsorbents using the Scherrer equation as previously mentioned, and the results are shown in Table 1.

Textural properties. The nitrogen sorption isotherms of the synthesized MOF adsorbents were recorded at 77 K, and the results are shown in Figure S8 and reveal type I isotherms as it is expected for materials with microporous nature. With different structural engineering techniques being used, the nitrogen uptake of the materials differed. First, the nitrogen uptake of UiO-66-0FA significantly increased when 200 equiv of formic acid was added to this synthesis mixture (UiO-66-200FA), which is the result of the creation of defects that render the structure more open and allow for better nitrogen sorption. However, although the functionalized structures were also synthesized with 200 equiv of formic acid, they all showed lower nitrogen sorption capacities than UiO-66-200FA. This is the result of the introduction of functional groups attached to the linker, which could partially block the porous network of the structure. However, depending on the bulkiness of the functional group attached, the nitrogen sorption levels of the functionalized structures differed, where UiO-66(NH_2) had the highest level followed by UiO-66$(OH)_2$ and then UiO-66$(COOH)_2$. Similarly, the nitrogen sorption of the MTV-MOFs was linked to the type and percent incorporation of the functionalized linkers. Moreover, samples functionalized with $(COOH)_2$ groups had lower nitrogen sorption than those functionalized with $(OH)_2$ groups for comparable percent

https://doi.org/10.1021/acsanm.2c02128
ACS Appl. Nano Mater. 2022, 5, 10795−10808

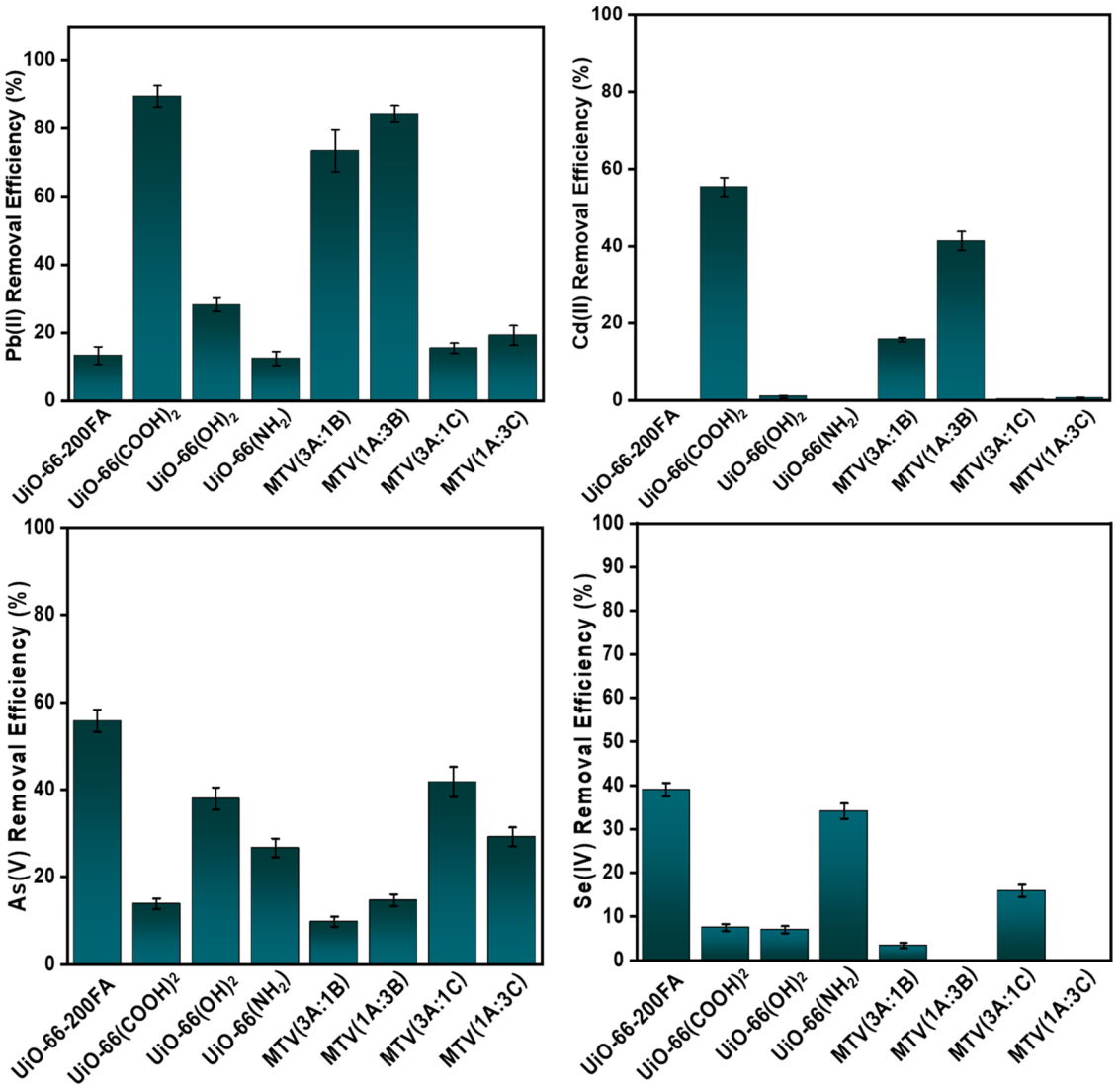

Figure 1. Bar graph showing the removal efficiency of each of all the MOF adsorbents as a percent of the initial contaminant concentration in the solution ($[Cd(II)]_0 = [Pb(II)]_0 = 14$ ppm; $[As(V)]_0 = [Se(IV)]_0 = 100$ ppm).

incorporation, while MTV-MOFs with lower percent incorporation had higher nitrogen sorption levels for the same functional group incorporated. Based on these observations, the Brunauer−Emmett−Teller (BET) surface area and pore volume of the different structures were calculated and are reported in Table 1.

Defect Number Estimation. To assess the thermal stability and estimate the defect number of the synthesized MOF adsorbents, TGA measurements were conducted, and the results are shown in Figure S9. The TGA curves shown in Figure S9 are normalized so that their final weight loss is at 100%, and this is to estimate the number of missing-linker defects in the structure based on a method reported in the literature.[55] The pure UiO-66 structures, namely UiO-66-0FA and UiO-66-200FA, showed better thermal stability than the fully functionalized structures as it is been reported before,[54] which is attributed to a lower metal−linker interaction in the case of functionalized structures.[26] Additionally, the thermal stability of the MTV-MOFs further confirmed the previous data, since structures with higher percent incorporation of functionalized linkers seemed to have slightly lower thermal stability. The defect number calculation was done based on a method reported in the literature,[55] with a few modifications to the method for the MTV-MOF structures,[26] and the results are depicted in Table 1. The addition of 200 equiv of formic acid to UiO-66-0FA increased its defects number from 1.36 to 1.87 missing linkers per cluster out of 6. The defect number of the functionalized structure fluctuated between 1.51 and 2.01 without a clear trend. Moreover, the defect number of the MTV-MOFs seemed to be higher in structures with higher percent incorporation of functionalized linkers, although it was not bounded between the defect numbers of the single-component counterparts.

Contaminant Removal from Water. *Screening of the Different Adsorbents Synthesized.* The full characterization of the MOFs synthesized provided a detailed description of their adsorption sites, both on their backbones and their cluster, and details on their porous network, surface area, particle size, and morphology. The aim was then to test the role of each one of these factors in the performance of UiO-66-based adsorbents for the decontamination of water from some of the most toxic pollutants. To gain a detailed understanding of the mechanism by which the adsorption is taking place, the contaminants chosen were two cations, Pb(II) and Cd(II), and two anions, As(V) and Se(IV). In the first stage of the study, a screening

https://doi.org/10.1021/acsanm.2c02128
ACS Appl. Nano Mater. 2022, 5, 10795−10808

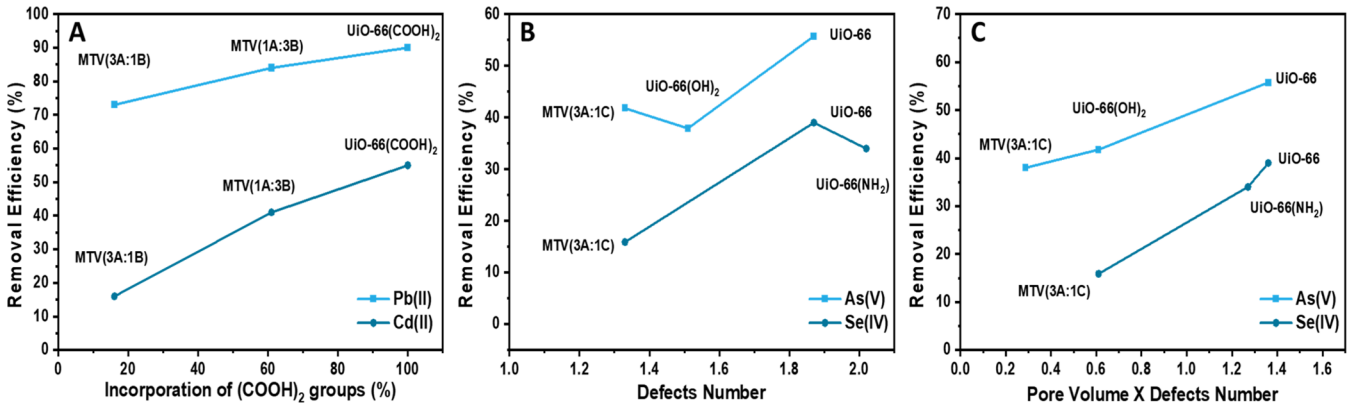

Figure 2. Correlations between the removal efficiency and various characteristics of the best-performing MOFs.

process was carried out to test the efficiency of every MOF synthesized using different structural engineering techniques in the removal of each one of the pollutants. To this end, a batch adsorption system was used where each MOF was added to a solution containing a given initial concentration of one of the contaminants, and the mixture was sealed and placed on a shaker overnight. The adsorption capacity of the different MOFs was measured as a percent adsorbed pollutant relative to its initial concentration. The best-performing MOFs were then used for a more detailed study. The screening process aimed to understand the role of the different characteristics of the UiO-66-based structures in the efficient decontamination of the different types of pollutants from water, and the results are shown in Figure 1 and Table S2.

Starting with the cations and specifically Pb(II) with an initial concentration of 14 ppm, it could be seen that three MOFs had by far the highest adsorption of Pb(II) cations, while other MOFs fell behind with significantly lower adsorption performances. The three best-performing MOFs were UiO-66-$(COOH)_2$, MTV(1A:3B), and MTV(3A:1B), with removal efficiencies of around 90, 84, and 73% respectively. The main difference between these structures and other counterparts is that they are all functionalized with $(COOH)_2$ groups, either fully as is the case for UiO-66$(COOH)_2$ or partially as is the case with MTV(1A:3B) and MTV(3A:1B), which have 61 and 16% incorporation of linkers functionalized with $(COOH)_2$ groups, respectively. This suggests that the carboxylate functional groups acted as efficient adsorption sites for the Pb(II) cations. Starting with a solution of water contaminated with Pb(II) and following the addition of the MOF, it is expected that the COOH groups of UiO-66$(COOH)_2$ exist in their deprotonated forms (COO^-).[56] Given the strong electron-accepting affinity of the Pb(II) cations, their interaction with COO^- becomes much stronger, which could explain the higher performance of UiO-66$(COOH)_2$.[56] The reason behind the synthesis and testing of the MTV-MOFs is that the fully functionalized UiO-66-$(COOH)_2$ has a much lower surface area than its counterparts caused by the bulky functional groups in the backbone of the framework, so MTV-MOFs with lower loading of these linkers were considered. The aim was to obtain structures that are partially functionalized with COOH groups but have higher surface areas, pore volume, and more accessible adsorption sites than the pure UiO-66$(COOH)_2$ to test if having a more open structure would lead to higher adsorption efficiency. On the contrary and as can be seen in Figure 1, it seems that the lower the percent incorporation of these functional groups, the lower the adsorption capacity. This proves that the COOH groups indeed acted as the adsorption sites of Pb(II) cations. Moreover, Pb(II) cations have a relatively small ionic diameter of 2.4 Å, and small ions have been associated with higher adsorption rates.[57] However, Pb(II) cations are hydrated in water and thus have a total diameter of 8.02 Å with their hydration shell, which might have hindered their diffusion into the UiO-66$(COOH)_2$ porous structure.[58] This could mean that most of the adsorption took place on the outer surface of the MOFs and not inside the porous structure, which marginalizes the effect of the surface area and pore volume of the MOFs and the ionic diameter of the pollutant.[59] This could be especially true given the small particle size of the UiO-66$(COOH)_2$ samples, as could be seen in the SEM images in Figure S7, which increases the level of the external surface area of the adsorbent relative to the internal one. Another possible scenario is the dehydration of Pb(II) ions, which could allow their diffusion in the UiO-66$(COOH)_2$ porous structure; in fact, the lower the hydration energy of a certain ion, the higher the possibility of it losing all, or part of, its hydration shell, increasing its adsorption. Pb(II) cations with 1502 KJ/mol hydration energy had been considered to be relatively easy to dehydrate, which could allow their diffusion in the porous network of UiO-66$(COOH)_2$ where more adsorption sites become accessible.[58]

The MOF that had the next best performance was UiO-66$(OH)_2$ followed by the MTV-MOFs that are partially functionalized with $(OH)_2$ groups, namely MTV(1A:3C) and MTV(3A:1C). Pb(II) cations, as Lewis acids, could coordinate with the OH groups, as they have a lone pair of electrons on their oxygen atoms, acting as a Lewis base.[60] This is also the expected mechanism when using UiO-66(NH_2) as an adsorbent, as it has a lone pair on the nitrogen atoms.[60] Regarding the MTV-MOFs, the higher the percent incorporation of $(OH)_2$ groups, the better the performance, validating the hypothesis that $(OH)_2$ groups are also acting as adsorption sites, although they have weaker interactions with Pb(II) than $(COOH)_2$ groups.

UiO-66 came next, and its adsorption capacity was attributed to the existence of structural defects as indicated before, which also seem to act as adsorption sites but with even lower interactions with Pb(II).[60]

When observing the removal efficiency of the different MOFs in the case of Cd(II) cations and starting with a concentration of 14 ppm as well, similar conclusions could be made. Moreover, being a cation with high electron-withdrawing capacity, it would be expected that Cd(II) will also have the strongest affinity toward UiO-66$(COOH)_2$ (55% Cd(II) removal efficiency) and

https://doi.org/10.1021/acsanm.2c02128
ACS Appl. Nano Mater. 2022, 5, 10795−10808

Scheme 2. Flow Chart Highlighting the Screening of the Different UiO-66-Based Structures in the Adsorption of Pb(II), Cd(II), As(V), and Se(IV)

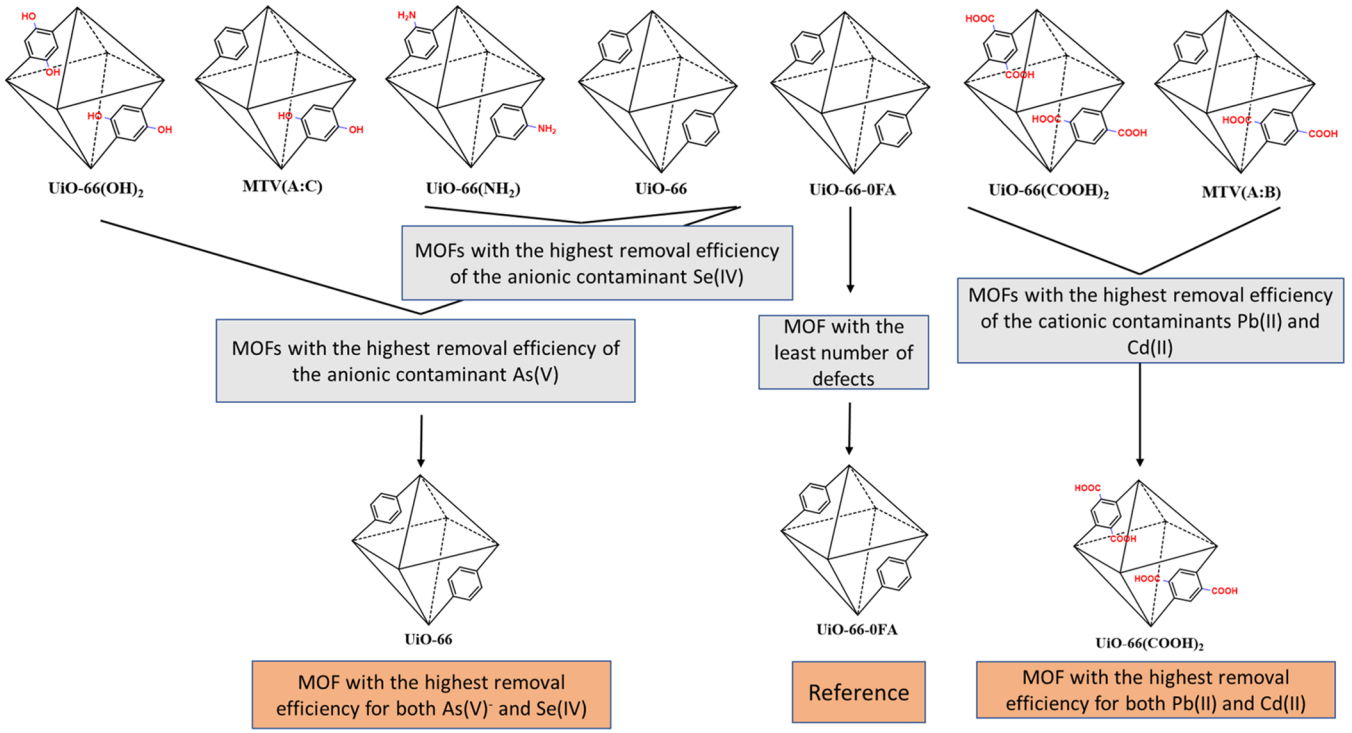

the MTV-MOFs functionalized with $(COOH)_2$ groups. In this case, too, MTV(1A:3B) (41% Cd(II) removal efficiency) performed better than MTV(3A:1B) (16% Cd(II) removal efficiency), since it had a higher percentage of $(COOH)_2$ groups. A linear correlation could be observed between the removal efficiency of the cations and the change in the percent incorporation of the COOH groups in the best-performing MOFs, as could be seen in Figure 2A. Moreover, the removal efficiency of Cd(II) was lower than that of Pb(II) using the same adsorbents. This could be explained by the bigger hydration diameter (8.52 Å) and higher hydration energy (1828 KJ/mol), which might have hindered the diffusion of Cd(II) into the porous network of the MOFs, meaning that the adsorption might have mostly taken place on the outer surface of the adsorbents.[58] However, MOFs with no COOH groups on their linkers did not seem to adsorb Cd(II) almost at all. This could be due to the lower absolute electronegativity of Cd(II) compared to that of Pb(II), which makes it harder to form stable complexes.[60] Following these results and given that the best-performing MOF in cation removal was by far UiO-66-$(COOH)_2$, the rest of the study on cation removal was performed using this MOF only, along with two UiO-66 samples as a reference (Scheme 2).

Moving on to the study on the removal of anions and starting with As(V) with an initial concentration of 100 ppm, it could be noticed from Figure 1 that the three best-performing MOFs were UiO-66, MTV(1A:3B) with 13% incorporation of $(OH)_2$-functionalized linkers, and UiO-66$(OH)_2$. Unlike the case of the cationic pollutants, the functionalization of the structures did not play a positive role in the removal efficiency of the MOF adsorbents in the case of As(V) anion removal. All the functionalized structures, fully or partially, had a lower removal efficiency than that of the pure UiO-66. Moreover, it had been previously reported that in the case of highly defected UiO-66 adsorbents, the As(V) anions adsorb on the defect sites of the Zr-clusters, which were induced by different modulation synthesis conditions.[48] In this study, the modulation synthesis procedure was followed, and 200 equiv of the formic acid modulator was added to the MOF synthesis solution to create defects in all structures, and the defect numbers are reported in Table 1. However, the trend in the removal efficiency of contaminants by the different MOF adsorbents was not directly proportional to the number of defects. This could indicate that these defects which act as adsorption sites were not all accessible.[61] The UiO-66 structure is known to have tetrahedral and octahedral pores of 8 and 11 Å diameters, respectively, and an aperture of 7 Å.[62] Moreover, the functionalization of the UiO-66 structure is expected to make the pore aperture smaller,[63] especially for bulkier functional groups attached to the linker such as COOH groups. Given that the arsenate anions are around 4.96 Å in diameter and around 9 Å with their hydration shell,[64] it is expected that the diffusion of these anions into the open structure of UiO-66 will be easier and faster than in the functionalized structure even if partial or total dehydration occurs. This is further confirmed by analyzing the results obtained using the MTV-MOFs where the structure with lower percent incorporation of $(OH)_2$ groups performed better, further proving that the functionalization of the UiO-66 structure might have caused partial inaccessibility of the adsorption sites. In addition to the pure UiO-66 structure, structures functionalized with $(OH)_2$ and NH_2 groups showed a comparable removal efficiency. Although part of the defect sites could be blocked by the presence of functional groups, having Lewis/Bronsted basic groups such as the hydroxyl or amino groups could enhance the removal of the arsenate anions by hydrogen bonding between the amine or hydroxyl groups and the negatively charged arsenate. This could be further confirmed by observing the results obtained for the Se(IV) (20 ppm initial

https://doi.org/10.1021/acsanm.2c02128
ACS Appl. Nano Mater. 2022, 5, 10795−10808

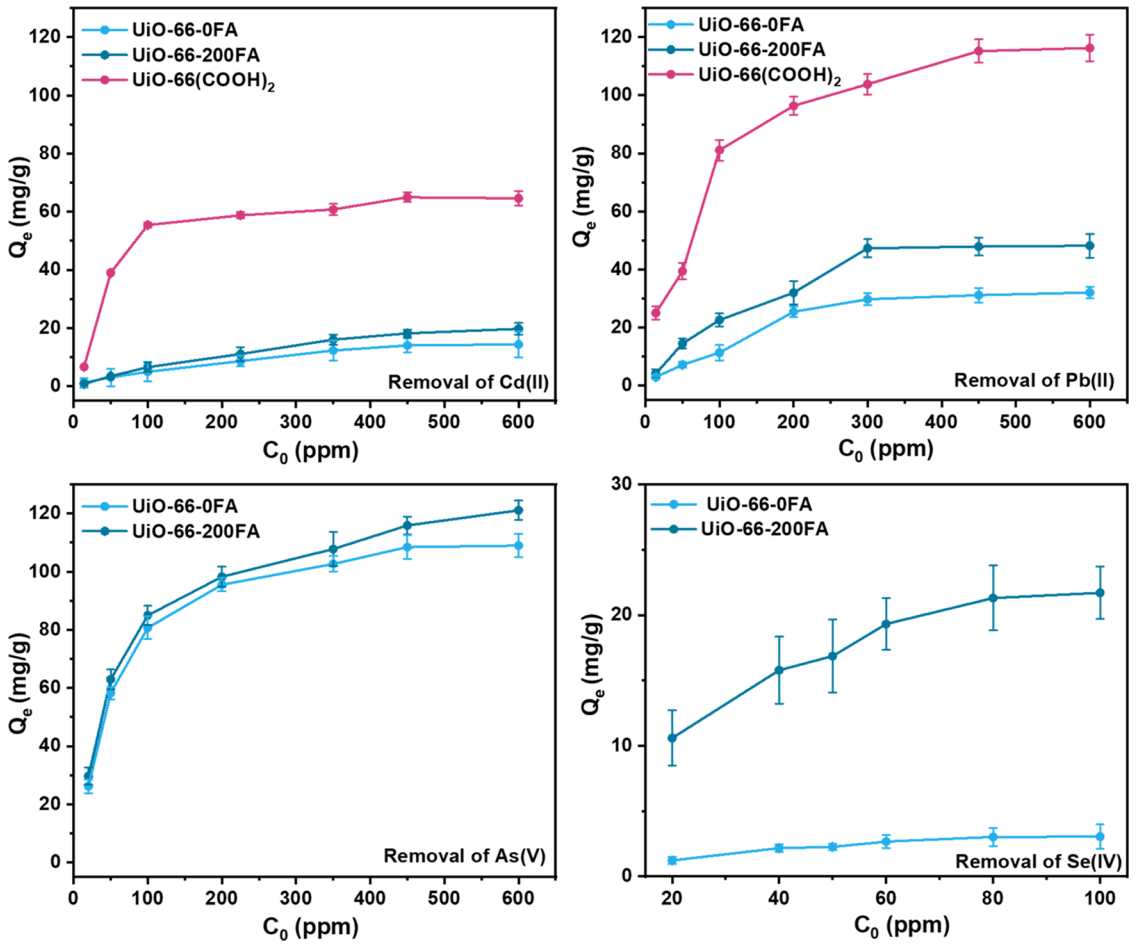

Figure 3. Adsorption isotherms of Pb(II) and Cd(II) onto UiO-66$(COOH)_2$ and of Pb(II), Cd(II), As(V), and Se(IV) onto UiO-66-200FA and UiO-66-0FA.

concentration) removal using the different MOF structures, where the best-performing MOFs were UiO-66, UiO-66(NH_2), and MTV(3A:1B) with 13% incorporation of $(OH)_2$ groups. Again, the removal efficiency was not directly proportional to the number of defects but rather to the accessibility of defect sites, which could be reflected by the higher surface area and pore volume. This means that the higher the pore volume and surface area or the lower the incorporation of bulky units, the better the adsorption of Se(IV) anions on the MOF defect sites. When plotting the removal efficiency of the anions using the three best-performing MOFs against their defect number, no clear correlation could be obtained (Figure 2B). However, a perfect linear correlation could be obtained when the removal efficiency is plotted against a factor obtained by the multiplication of the defect number by the pore volume, thus considering the accessibility of those defect sites by the anions (Figure 2C). Moreover, given the 5.2 Å ionic diameter of the Se(IV) anions, it would be expected that the diffusion of these anions would be easier in the open UiO-66 structure and rather limited when the internal porous network is blocked by bulky functional groups.[61] This would be especially hindering the adsorption in the case where the functional groups on the linker are not effective adsorption sites. The exception here is UiO-66(NH_2), which seemed to have comparable performance to that of UiO-66 since the NH_2 groups seemed to form hydrogen bond interactions with the Se(IV) anions, making them adsorption sites themselves. In the case of anion removal from water, UiO-66-200FA showed the best performance in the screening process, so the rest of the study will be focused on it, while UiO-66-0FA will be used as a reference (Scheme 2).

Following the initial adsorption studies, the best-performing MOF adsorbents were collected from the contaminated solutions, dried, and analyzed again using FTIR, PXRD, and SEM imaging to gain some insights into the adsorption sites and to assess their chemical stabilities. The results are shown in Figures S10−S12 in the Supporting Information. The FTIR spectra of the best-performing MOFs (UiO-66-200FA and UiO-66$(COOH)_2$) before and after adsorption of the contaminants were recorded, and the results are shown in Figure S10. We noticed that the characteristic peaks of UiO-66-200FA at 661 and 747 cm^{-1} (attributed to the stretch vibration of O−H and Zr−O clusters, respectively)[57] in addition to the peaks at 1398, 1506, and 1577 cm^{-1} (attributed to the stretch vibration of the −COOH groups linked to the zirconium centers) remained well-matched together before and after adsorption of Se(IV) and As(V).[24,65] This implied the formation of outer-sphere complexes between the parent MOF and the anionic contaminants characterized by strong chemical interactions and no alteration in the chemical structure of the framework. Moreover, while no disappearance or addition of new bands was observed in the case of UiO-66$(COOH)_2$ when comparing the characteristic peaks at 652, 1384, 1429, and 1590 cm^{-1}, the band at 1660 cm^{-1} which is a characteristic of the free −COOH groups in the MOF decreased after Pb(II) adsorption and

https://doi.org/10.1021/acsanm.2c02128
ACS Appl. Nano Mater. 2022, 5, 10795−10808

almost disappeared in the case of Cd(II) adsorption, suggesting the coordination of the free -COO^- groups with the two studied metal cations through strong chemical bonds.[65] The PXRD patterns of the used adsorbents match the patterns of the fresh MOF samples, which demonstrate that the MOF structures preserved their crystallinity following the adsorption of the contaminants. Moreover, a narrow 2θ range of the PXRD patterns is also displayed in Figure S11 in the Supporting Information, and it reveals a shift of the characteristic peaks toward a higher value upon the adsorption of Pb(II), Cd(II), As(V), and Se(IV). This interesting observation could be due to the introduction of the pollutant species inside the porous structure of the MOF adsorbents, which might have cell expansion in the structure.[53,54] This shift in the peaks is gradual and proportional to the pollutants' ionic radii, where the higher this diameter, the bigger the tensile stress this pollutant introduces to the structure upon its adsorption and the higher the shift in the peak relative to the pure structures. Additionally, the SEM images of the best-performing MOFs following the adsorption of pollutants were recorded, and the results are shown in Figure S12. Comparing the images before and after adsorption, it could be seen that the morphology of the crystals remains intact, which further confirms the stability of these structures under the experimental conditions used in the adsorption study. Finally, SEM-EDX images shown in Figures S13−S22 reveal the presence of the pollutants on the MOF adsorbents. Additionally, it confirms the previously discussed trend where the adsorption of cations increases with the introduction of $(COOH)_2$ functional groups and where the adsorption of anions increases with the increase in the number of defects of the pure UiO-66 structure.

To assess the pollutant desorption and adsorbent recycling efficiency over many cycles, the best-performing MOFs were washed and reused as adsorbents for four consecutive cycles, and the results are shown in Figure S23. The results obtained indicated that both UiO-66$(COOH)_2$ and UiO-66-200FA adsorbents can be effectively regenerated and reused in the Pb(II), Cd(II), As(V), and Se(IV) removal from water with no significant decrease in the adsorption capacity during the four cycles of regeneration.

Adsorption Isotherms. To understand the nature of the interactions between the MOF adsorbents and the different adsorbates, the adsorption capacity of the most effective MOFs (UiO-66-200FA and UiO-66$(COOH)_2$) was further studied at different pollutant concentrations as shown in Figure 3. UiO-66-0FA was also employed in this set of experiments as a reference. As expected, the common observation in all studies is that the adsorption capacity Q_e (mg/g) of all MOFs increases with the increase in the initial concentration of the corresponding contaminant C_0 (ppm) to reach a plateau at higher C_0 in all isotherms. This is due to reaching the maximum adsorption capacity of the MOFs, as most adsorption sites become occupied with the further increase of contaminant ion concentration.

Additionally, in all studies performed, UiO-66-200FA has a higher adsorption capacity than that of UiO-66-0FA, which is attributed to an increase in the number of defects and subsequently the increase in the density of adsorption sites, surface area, and pore volume. This is especially obvious in the adsorption of Se(IV) anions where the adsorption capacity dropped significantly when the number of defects decreased upon using UiO-66-0FA instead of UiO-66-200FA. It is important to note here that the decrease in the number of defects is not only reflected by a decrease in the number of active sites but also a decrease in the surface area and pore volume of the structure (Table 1), which makes the diffusion of Se(IV) anions and the accessibility of active sites harder in UiO-66-0FA. In the case of cation adsorption, it could be seen that for all the values of C_0, the adsorption capacity is significantly higher in the case of UiO-66$(COOH)_2$ adsorbents than it is for both UiO-66-200FA and UiO-66-0FA. This further confirms the importance of the functionalization of UiO-66 with $(COOH)_2$ groups as a strategy to boost the adsorption capacity toward cationic HMIs.

To better understand the nature of the interaction between the chemical pollutants and the MOF adsorbents, the adsorption isotherm data were fitted into adsorption models, namely the linear-form Langmuir model and Freundlich model presented in the Supporting Information.

The results for the data fitting using both models for the contaminants using the most efficient MOF adsorbents are shown in Figure S24 in the Supporting Information. The assumption based on which the Langmuir model was developed is that the adsorption sites are equal in accessibility and energy, which results in monolayer adsorption of the adsorbates on the surface of the adsorbents. However, it is assumed in the Freundlich model that the adsorption causes the formation of multilayers of the adsorbate on the surface of the adsorbent, which is nonuniform and heterogeneous, and that the process is irreversible and nonideal.

As could be seen from the fitting results in Figure S24 and from the R^2 values corresponding to each model, the Langmuir model represents a better fit of the adsorption isotherms. Thus, the adsorption of the cations onto UiO-66$(COOH)_2$ and that of the anions onto UiO-66 are better described as a monolayer adsorption process.

Q_{max} of adsorption of the different pollutants using the UiO-66-based adsorbents was calculated following fitting the adsorption isotherms using the Langmuir model, and the results are shown in Table 2. In all the studies performed, the reference

Table 2. Q_{max} (mg/g) Obtained Using the UiO-66-Based Adsorbents for the Removal of Pb(II), Cd(II), As(V), and Se(IV)

	Pb(II)	Cd(II)	As(V)	Se(IV)
UiO-66$(COOH)_2$	125.2	69.1		
UiO-66-200FA	66.7	34.8	132.5	30.8
UiO-66-0FA	49.3	23.8	113.3	5.0

adsorbent UiO-66-0FA had the lowest Q_{max}, further confirming previous conclusions on the role of defects and/or the carboxyl functional groups on the linker as adsorption sites. This is further confirmed in previous studies that showed the effect of the increase in the defect number on the increased Pb(II) adsorption in UiO-66 adsorbents.[65] In fact, the UiO-66-0FA sample shows a similar Q_{max} of Pb(II) compared to previously synthesized UiO-66 samples with HCl as a modulator (48.7 mg/g),[66] while it performed much better than a sample synthesized to have as little as 0.1 defects per cluster (19.4−25.5 mg/g).[65] On the other hand, UiO-66 samples with a higher defect number than that of UiO-66-200FA show higher Pb(II) adsorption capacities that could reach 175.6 mg/g for 2.3 defects per cluster.[65] This further confirms that defects influence the adsorption of cationic pollutants. However, compared to UiO-66-200FA, Q_{max} of adsorption of Pb(II) and Cd(II) using UiO-66$(COOH)_2$ was almost two times higher. Although the defect sites contributed to the adsorption of the cationic pollutants, the

https://doi.org/10.1021/acsanm.2c02128
ACS Appl. Nano Mater. 2022, 5, 10795−10808

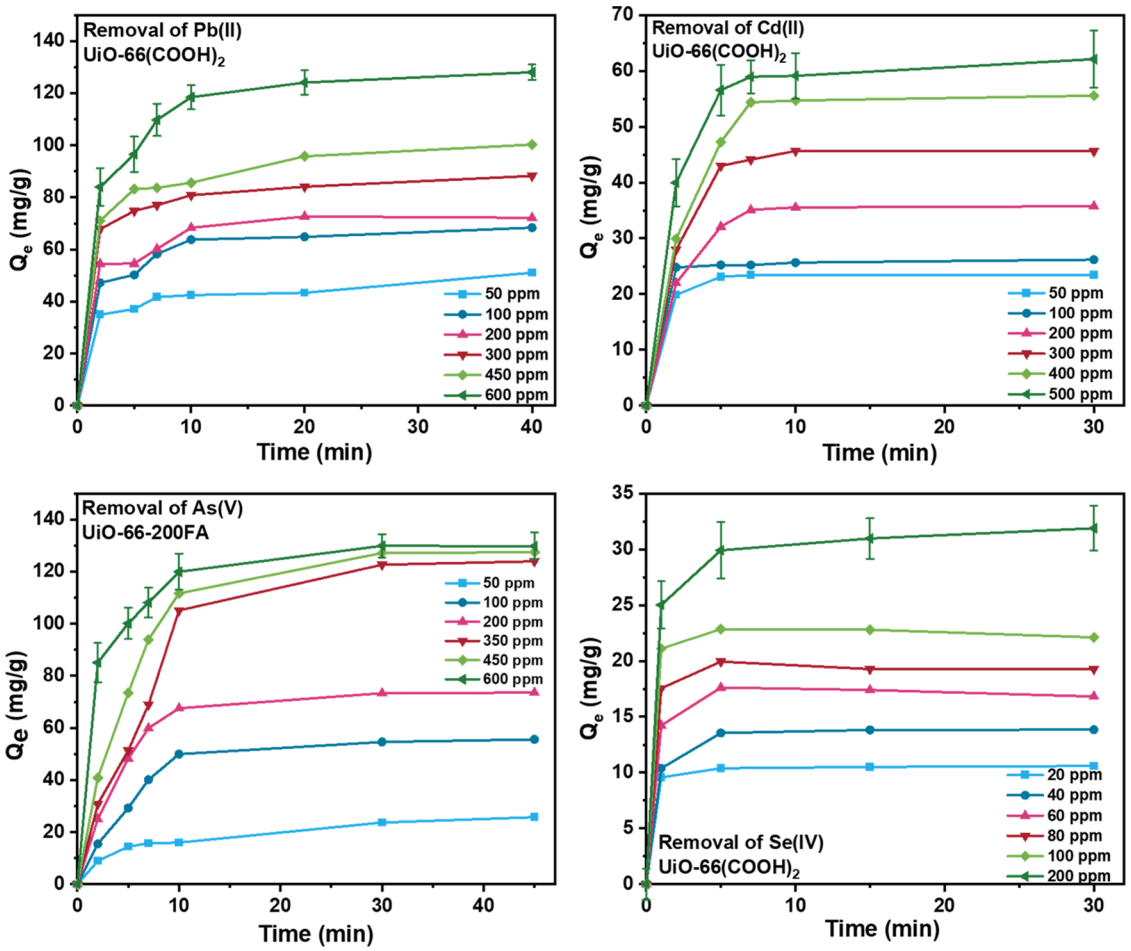

Figure 4. Uptake of Pb(II) and Cd(II) onto UiO-66(COOH)2 and Pb(II), Cd(II), As(V), and Se(IV) onto UiO-66 starting with various initial concentrations of the pollutants and as a function of the contact time.

carboxyl functional groups played the main role in the removal of Pb(II) and Cd(II). This is in agreement with previous reports in the literature where UiO-66 functionalized with sulfonic acid groups (SO_3H) yielded around 3.6 times higher Cd(II) adsorption than UiO-66, reaching as high as 409.96 mg/g.[67] In this study as well, the authors attribute the higher Cd(II) adsorption capacity to the SO_3H groups that are the preferred binding sites. On the other hand, while little adsorption of As(V) and Se(IV) occurred when using UiO-66$(COOH)_2$, Q_{max} using UiO-66-200FA as an adsorbent was calculated as 132.5 and 30.8 mg/g, respectively. Since defects were the main adsorption sites for the anionic pollutants, UiO-66-0FA showed a relatively good Q_{max} of adsorption of As(V), as it has defects as well but with a lower defect number compared to that of UiO-66-200FA. In fact, it has been previously reported that the defect cluster of UiO-66 makes excellent binding sites for As(V), where a higher Q_{max} (303 mg/g) was obtained at pH = 2 and after 2880 min of adsorption.[68] As for the adsorption of Se(IV), the lower surface area of UiO-66-0FA and the higher molecular radii of Se(IV) resulted in a low Q_{max} of adsorption in this case compared to that of UiO-66-200FA. Different synthesis and testing conditions of UiO-66 adsorbents yielded a higher Q_{max} of adsorption of Se(IV) (59.9 mg/g),[46] further highlighting the effect of the structural engineering of this highly tunable MOF on its properties and efficiency in adsorption applications.

Adsorption kinetics. The adsorption kinetics of Pb(II) and Cd(II) onto UiO-66$(COOH)_2$ and that of As(V) and Se(IV) onto UiO-66-200FA as a function of the contact time were investigated, and the results are shown in Figure 4. For all the pollutants studied and for any given time, Q_e increases with the increase in the pollutant starting concentration, which could be explained again by the increased mass transfer, allowing for higher adsorption. Additionally, the adsorption undergoes two distinct phases; the first is very fast at the beginning for the first ten minutes, and then, it is a slower phase until the adsorption reaches a plateau. This highlights the efficiency of the UiO-66-based MOFs for practical applications in pollutant removal from the water where the adsorption equilibrium is reached within minutes. The kinetic data were analyzed by fitting them using two kinetic models, pseudo-first-order and pseudo-second-order, that are represented in the Supporting Information.

The fitting data are shown in Figure S25 in the Supporting Information. Figure S25 clearly shows that the pseudo-second-order model makes a better representation of the kinetic data obtained for all the pollutant−adsorbent combinations studied. The pseudo-second-order kinetic model assumes that chemical adsorption is the dominant mechanism, even in the presence of physical interactions between the adsorbent and the adsorbate. This means that in all the kinetic experiments, chemisorption was the predominant type of interaction between the adsorbents and the UiO-66-based adsorbents.

Detailed Mechanism for Most Effective MOFs. Based on the data from the screening process and the adsorption isotherms and kinetic models, plausible mechanisms for the adsorption of

https://doi.org/10.1021/acsanm.2c02128
ACS Appl. Nano Mater. 2022, 5, 10795−10808

both the anions and cations by the MOF adsorbents are suggested. Starting with the adsorption of the metal cations Pb(II) and Cd(II) onto UiO-66(COOH)$_2$, the suggested binding mechanisms are shown in Scheme 3, where both Pb(II) and Cd(II) are represented as M^{2+}. The metal cations could form coordination complexes with the COOH functional groups as is the case in the mechanisms labeled 2 and 5 in Scheme 3. Another form of interaction would involve the direct bonding between the free hydroxyl groups and the metal cations as is the case in the mechanisms labeled 3 and 4. Additionally, cation−π interactions could also take place between the metal cations and the π electron cloud of the aromatic linker in a UiO-66-based structure, as is shown in the mechanism labeled 1, which is a type of physisorption.[47]

Scheme 3. Labels 1−5 Indicate the Different Potential Adsorption Mechanisms of Pb(II) or Cd(II) Cations, Represented as M^{2+}, on UiO-66(COOH)$_2$ Adsorbents

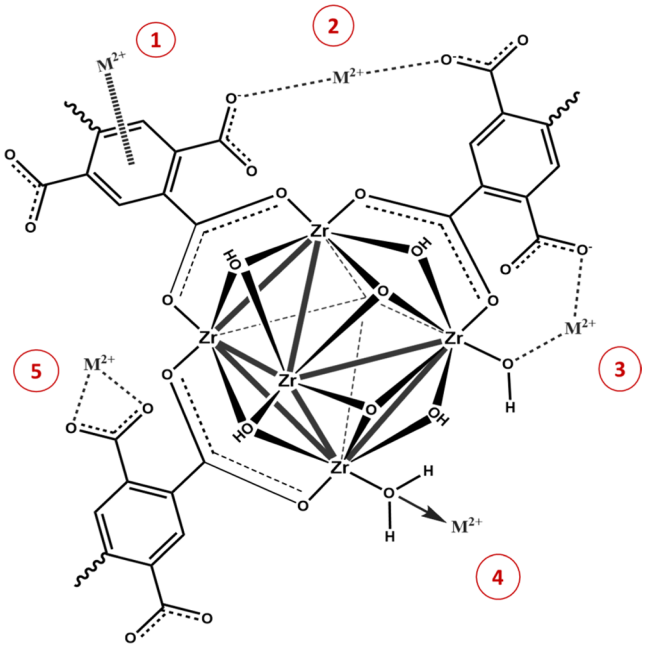

As for the anions, the possible and suggested adsorption mechanisms onto the defect UiO-66-200FA are represented in Scheme 4 separately for As(V) and Se(IV). In a defect-free Zr-cluster site where a BDC linker exists, the adsorption site would be the Zr-OH groups, as shown in the mechanisms labeled 2 and 4 for As(V) and Se(IV), respectively, in Scheme 4. In this case, the anions act as acid-binding sites to hydroxyl groups, forming complexes with the Zr-cluster as illustrated.[69] However, in the presence of defects, the preferred binding mechanism of the anions on the Zr-cluster would be through the defect site by forming single or double coordination, as shown in the mechanisms labeled 1 and 3 for the As(V) anions and that labeled 5 for Se(IV).[48,61]

CONCLUSIONS

In summary, a series of nine UiO-66-based adsorbents were synthesized with high defect numbers and different functionalities and were tested as adsorbents for the removal of highly toxic cationic (Pb(II) and Cd(II)) and anionic (As(V) and Se(IV)) pollutants from water. The best-performing MOF for the cation removal was the structure fully functionalized with carboxylate groups, UiO-66(COOH)$_2$, and the removal efficiency seemed to be linearly correlated with the percent incorporation of these functional groups in the structure. On the other hand, the Zr-cluster defects were believed to be the preferred adsorption sites for anionic pollutants. The accessibility of these adsorption sites on the cluster was hindered by the functionalization of the structure, making the nonfunctionalized and high-defect UiO-66-200FA the best-performing MOF for the removal of anions. The adsorption isotherms and the adsorption kinetics were characterized for the best-performing members, and the data fitting in different models helped conclude that the predominant adsorption mode was monolayer chemisorption, and different adsorption mechanisms were suggested on the different structures. The adsorption equilibrium was reached within minutes for all adsorbents used, highlighting the potential of using MOFs as adsorbents in real-life applications. Finally, this is the first study of a wide variety of UiO-66-based structures without further postsynthetic mod-

Scheme 4. Labels 1−3 and 4−5 Indicate the Potential Adsorption Mechanisms of As(V) and Se(IV) Anions, Respectively, onto High-Defect UiO-66 Adsorbents

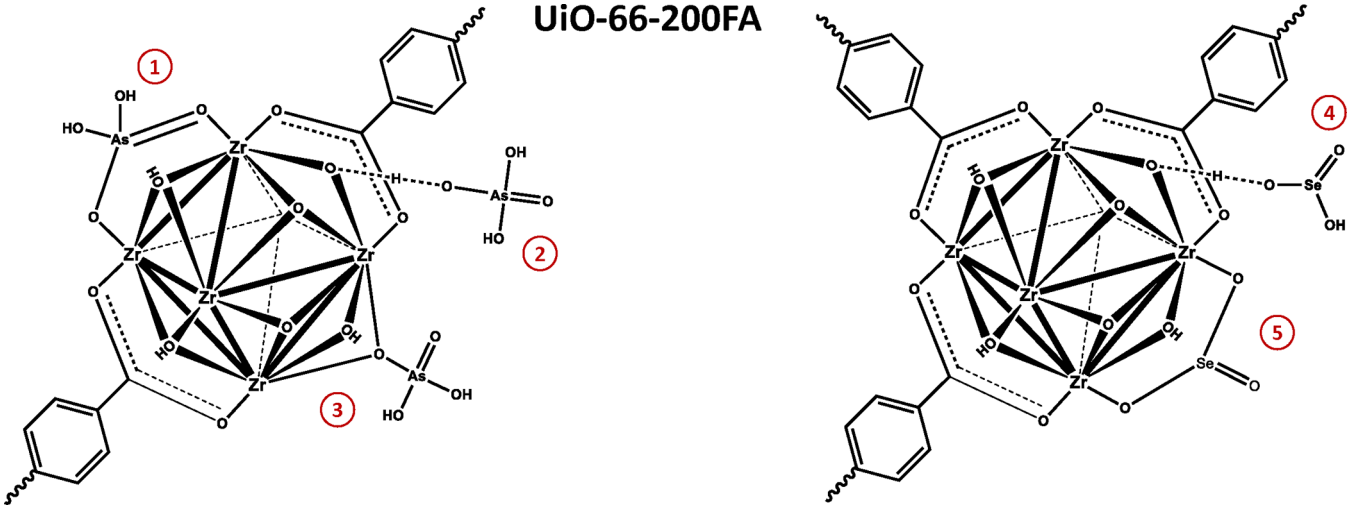

https://doi.org/10.1021/acsanm.2c02128
ACS Appl. Nano Mater. 2022, 5, 10795−10808

ifications for the removal of a range of chemical pollutants. The study helps to give a comprehensive conclusion on the structural engineering required for both the cluster and linker to maximize the performance of these materials for the decontamination of wastewater from highly toxic compounds.

■ ASSOCIATED CONTENT

Supporting Information

The Supporting Information is available free of charge at https://pubs.acs.org/doi/10.1021/acsanm.2c02128.

Materials, detailed synthesis procedure, PXRD, narrow-range PXRD, proton NMR, SEM, textural properties, TGA, removal efficiency, FTIR, PXRD after adsorption, SEM after adsorption, SEM-EDX after adsorption, Q_e after four regeneration cycles, Langmuir and Freundlich models, and fitting figures (PDF)

■ AUTHOR INFORMATION

Corresponding Authors

Mohammad Ahmad − *Bahaa and Walid Bassatne Department of Chemical Engineering and Advanced Energy, Faculty of Engineering and Architecture, American University of Beirut, Beirut 1107 2020, Lebanon*; Email: ma258@aub.edu.lb

Mohamad Hmadeh − *Department of Chemistry, Faculty of Arts and Sciences, American University of Beirut, Beirut 1107 2020, Lebanon; Department of Chemistry, University of Toronto, Toronto, Ontario M5S 3H6, Canada*; orcid.org/0000-0003-3027-3192; Email: mohamad.hmadeh@aub.edu.lb

Authors

Asmaa Jrad − *Bahaa and Walid Bassatne Department of Chemical Engineering and Advanced Energy, Faculty of Engineering and Architecture, American University of Beirut, Beirut 1107 2020, Lebanon; NYUAD Water Research Center, New York University Abu Dhabi, Abu Dhabi 129188, United Arab Emirates*

Patrick Damacet − *Department of Chemistry, Faculty of Arts and Sciences, American University of Beirut, Beirut 1107 2020, Lebanon*

Zahraa Yaghi − *Department of Chemistry, Faculty of Arts and Sciences, American University of Beirut, Beirut 1107 2020, Lebanon*

Complete contact information is available at: https://pubs.acs.org/10.1021/acsanm.2c02128

Author Contributions

⊥A.J. and P.D. contributed equally to this work.

Notes

The authors declare no competing financial interest.

■ ACKNOWLEDGMENTS

M.H. acknowledges the support of the Arab Fund Fellowship Program. The authors gratefully acknowledge the funding provided by the American University of Beirut Research Board and the K. Shair Central Research Science Laboratory.

■ REFERENCES

(1) Barakat, M. A. New trends in removing heavy metals from industrial wastewater. *Arabian J. Chem.* **2011**, *4*, 361−377.

(2) Barrett, J. R. Chemical contaminants in drinking water: where do we go from here? *Environ. Health Perspect.* **2014**, *122*, A80.

(3) Antunes, M.; Teixeira, R.; Albuquerque, T.; Valente, T.; Carvalho, P.; Santos, A. Water-Rock Interaction and Potential Contamination Risk in a U-Enriched Area. *Geosciences* **2021**, *11*, 217.

(4) Bayabil, H. K.; Teshome, F. T.; Li, Y. C. Emerging Contaminants in Soil and Water. *Front. Environmen. Sci.* **2022**, *10*, No. 873499.

(5) Rathi, B. S.; Kumar, P. S.; Vo, D.-V. N. Critical review on hazardous pollutants in water environment: Occurrence, monitoring, fate, removal technologies and risk assessment. *Sci. Total Environ.* **2021**, *797*, No. 149134.

(6) Chaudhary, V. K.; Singh, S. K.; Srivastav, A. L.; Singh, A.; Patel, N.; Patel, A. Chapter 11 - Chemical water contaminants: potential risk to human health and possible remediation. In *Contamination of Water*, Ahamad, A.; Siddiqui, S. I.; Singh, P., Eds.; Academic Press, 2021; pp 157−172.

(7) Kumar, R.; Qureshi, M.; Vishwakarma, D. K.; Al-Ansari, N.; Kuriqi, A.; Elbeltagi, A.; Saraswat, A. A review on emerging water contaminants and the application of sustainable removal technologies. *Case Stud. Chem. Environ. Eng.* **2022**, *6*, No. 100219.

(8) Norton-Brandão, D.; Scherrenberg, S. M.; van Lier, J. B. Reclamation of used urban waters for irrigation purposes − A review of treatment technologies. *J. Environ. Manage.* **2013**, *122*, 85−98.

(9) Azimi, A.; Azari, A.; Rezakazemi, M.; Ansarpour, M. Removal of Heavy Metals from Industrial Wastewaters: A Review. *ChemBioEng Rev.* **2017**, *4*, 37−59.

(10) Ali, I. New Generation Adsorbents for Water Treatment. *Chem. Rev.* **2012**, *112*, 5073−5091.

(11) Al-Ghouti, M. A.; Li, J.; Salamh, Y.; Al-Laqtah, N.; Walker, G.; Ahmad, M. N. M. Adsorption mechanisms of removing heavy metals and dyes from aqueous solution using date pits solid adsorbent. *J. Hazard. Mater.* **2010**, *176*, 510−520.

(12) Salameh, Y.; Albadarin, A. B.; Allen, S.; Walker, G.; Ahmad, M. N. M. Arsenic(III,V) adsorption onto charred dolomite: Charring optimization and batch studies. *Chem. Eng. J.* **2015**, *259*, 663−671.

(13) Pradeep, T.; Anshup. Noble metal nanoparticles for water purification: A critical review. *Thin Solid Films* **2009**, *517*, 6441−6478.

(14) Erdem, E.; Karapinar, N.; Donat, R. The removal of heavy metal cations by natural zeolites. *J. Colloid Interface Sci.* **2004**, *280*, 309−314.

(15) Eddaoudi, M.; Moler, D. B.; Li, H.; Chen, B.; Reineke, T. M.; O'Keeffe, M.; Yaghi, O. M. Modular chemistry: secondary building units as a basis for the design of highly porous and robust metal-organic carboxylate frameworks. *Acc. Chem. Res.* **2001**, *34*, 319−330.

(16) Li, X.; Wang, B.; Cao, Y.; Zhao, S.; Wang, H.; Feng, X.; Zhou, J.; Ma, X. Water Contaminant Elimination Based on Metal−Organic Frameworks and Perspective on Their Industrial Applications. *ACS Sustainable Chem. Eng.* **2019**, *7*, 4548−4563.

(17) Furukawa, H.; Cordova, K. E.; O'Keeffe, M.; Yaghi, O. M. The Chemistry and Applications of Metal-Organic Frameworks. *Science* **2013**, *341*, 1230444.

(18) Kuppler, R. J.; Timmons, D. J.; Fang, Q.-R.; Li, J.-R.; Makal, T. A.; Young, M. D.; Yuan, D.; Zhao, D.; Zhuang, W.; Zhou, H.-C. Potential applications of metal-organic frameworks. *Coord. Chem. Rev.* **2009**, *253*, 3042−3066.

(19) Yaghi, O. M.; O'Keeffe, M.; Ockwig, N. W.; Chae, H. K.; Eddaoudi, M.; Kim, J. Metal−organic frameworks for heavy metal removal from water: Reticular synthesis and the design of new materials. *Nature* **2003**, *423*, 705−714.

(20) Chatterjee, Amrita.; H, X.; Lam, Frank. Leung.-Yuk. Towards a recyclable MOF catalyst for efficient production of furfural. *Catal. Today* **2018**, *314*, 129−136.

(21) Mortada, B.; Matar, T. A.; Sakaya, A.; Atallah, H.; Kara Ali, Z.; Karam, P.; Hmadeh, M. Postmetalated Zirconium Metal Organic Frameworks as a Highly Potent Bactericide. *Inorg. Chem.* **2017**, *56*, 4739−4744.

(22) Kobielska, P. A.; Howarth, A. J.; Farha, O. K.; Nayak, S. Metal−organic frameworks for heavy metal removal from water. *Coord. Chem. Rev.* **2018**, *358*, 92−107.

(23) Li, B.; Wen, H. M.; Zhou, W.; Chen, B. Porous Metal-Organic Frameworks for Gas Storage and Separation: What, How, and Why? *J. Phys. Chem. Lett.* **2014**, *5*, 3468−3479.

(24) Duan, C.; Zhang, H.; Li, F.; Xiao, J.; Luo, S.; Xi, H. Hierarchically porous metal−organic frameworks: rapid synthesis and enhanced gas storage. *Soft Matter* **2018**, *14*, 9589−9598.
(25) Jrad, A.; Hmadeh, M.; Abu Tarboush, B. J.; Awada, G.; Ahmad, M. Structural engineering of Zr-based metal-organic framework catalysts for optimized biofuel additives production. *Chem. Eng. J.* **2020**, *382*, No. 122793.
(26) Jrad, A.; Hmadeh, M.; Awada, G.; Chakleh, R.; Ahmad, M. Efficient biofuel production by MTV-UiO-66 based catalysts. *Chem. Eng. J.* **2021**, *410*, No. 128237.
(27) Van de Voorde, B.; Bueken, B.; Denayer, J.; De Vos, D. Adsorptive separation on metal−organic frameworks in the liquid phase. *Chem. Soc. Rev.* **2014**, *43*, 5766−5788.
(28) Adil, K.; Belmabkhout, Y.; Pillai, R. S.; Cadiau, A.; Bhatt, P. M.; Assen, A. H.; Maurin, G.; Eddaoudi, M. Gas/vapour separation using ultra-microporous metal−organic frameworks: insights into the structure/separation relationship. *Chem. Soc. Rev.* **2017**, *46*, 3402−3430.
(29) Zhuang, J.; Kuo, C.-H.; Chou, L.-Y.; Liu, D.-Y.; Weerapana, E.; Tsung, C.-K. Optimized Metal−Organic-Framework Nanospheres for Drug Delivery: Evaluation of Small-Molecule Encapsulation. *ACS Nano* **2014**, *8*, 2812−2819.
(30) Wang, L.; Zheng, M.; Xie, Z. Nanoscale metal−organic frameworks for drug delivery: a conventional platform with new promise. *J. Mater. Chem. B* **2018**, *6*, 707−717.
(31) Wang, Y.; Lin, S.; Luo, J.; Huang, R.; Cai, H.; Yan, W.; Yang, H. A Novel Tb@Sr-MOF as Self-Calibrating Luminescent Sensor for Nutritional Antioxidant. *Nanomaterials* **2018**, *8*, 796.
(32) Jia, L.; Guo, S.; Xu, J.; Chen, X.; Zhu, T.; Zhao, T. A Ratiometric Fluorescent Nano-Probe for Rapid and Specific Detection of Tetracycline Residues Based on a Dye-Doped Functionalized Nano-scaled Metal−Organic Framework. *Nanomaterials* **2019**, *9*, 976.
(33) Sava Gallis, D. F.; Rohwer, L. E. S.; Rodriguez, M. A.; Barnhart-Dailey, M. C.; Butler, K. S.; Luk, T. S.; Timlin, J. A.; Chapman, K. W. Multifunctional, Tunable Metal−Organic Framework Materials Platform for Bioimaging Applications. *ACS Appl. Mater. Interfaces* **2017**, *9*, 22268−22277.
(34) Wang, H.-S. Metal−organic frameworks for biosensing and bioimaging applications. *Coord. Chem. Rev.* **2017**, *349*, 139−155.
(35) Escorihuela, J.; Sahuquillo, Ó.; García-Bernabé, A.; Giménez, E.; Compañ, V. Phosphoric Acid Doped Polybenzimidazole (PBI)/Zeolitic Imidazolate Framework Composite Membranes with Significantly Enhanced Proton Conductivity under Low Humidity Conditions. *Nanomaterials* **2018**, *8*, 775.
(36) Muñoz-Gil, D.; Figueiredo, F. M. L. High Surface Proton Conduction in Nanostructured ZIF-8. *Nanomaterials* **2019**, *9*, 1369.
(37) Efome, J. E.; Rana, D.; Matsuura, T.; Lan, C. Q. Experiment and modeling for flux and permeate concentration of heavy metal ion in adsorptive membrane filtration using a metal-organic framework incorporated nanofibrous membrane. *Chem. Eng. J.* **2018**, *352*, 737−744.
(38) Efome, J. E.; Rana, D.; Matsuura, T.; Lan, C. Q. Insight Studies on Metal-Organic Framework Nanofibrous Membrane Adsorption and Activation for Heavy Metal Ions Removal from Aqueous Solution. *ACS Appl. Mater. Interfaces* **2018**, *10*, 18619−18629.
(39) Efome, J. E.; Rana, D.; Matsuura, T.; Lan, C. Q. Metal−organic frameworks supported on nanofibers to remove heavy metals. *J. Mater. Chem. A* **2018**, *6*, 4550−4555.
(40) Abdelhameed, R. M.; Emam, H. E. Modulation of metal organic framework hybrid cotton for efficient sweeping of dyes and pesticides from wastewater. *Sustainable Mater. Technol.* **2022**, *31*, No. e00366.
(41) Emam, H. E.; El-Shahat, M.; Abdelhameed, R. M. Observable removal of pharmaceutical residues by highly porous photoactive cellulose acetate@MIL-MOF film. *J. Hazard. Mater.* **2021**, *414*, No. 125509.
(42) Abdelhameed, R. M.; Abdel-Gawad, H.; Emam, H. E. Macroporous Cu-MOF@cellulose acetate membrane serviceable in selective removal of dimethoate pesticide from wastewater. *J. Environ. Chem. Eng.* **2021**, *9*, No. 105121.
(43) Cavka, J. H.; Jakobsen, S.; Olsbye, U.; Guillou, N.; Lamberti, C.; Bordiga, S.; Lillerud, K. P. A New Zirconium Inorganic Building Brick Forming Metal Organic Frameworks with Exceptional Stability. *J. Am. Chem. Soc.* **2008**, *130*, 13850−13851.
(44) Lee, Y.-R.; Kim, J.; Ahn, W.-S. Synthesis of Metal-Organic Frameworks: A Mini Review. *Korean J. Chem. Eng.* **2013**, *30*, 1667−1680.
(45) Kandiah, M.; Nilsen, M. H.; Usseglio, S.; Jakobsen, S.; Olsbye, U.; Tilset, M.; Larabi, C.; Quadrelli, E. A.; Bonino, F.; Lillerud, K. P. Synthesis and Stability of Tagged UiO-66 Zr-MOFs. *Chem. Mater.* **2010**, *22*, 6632−6640.
(46) Wei, J.; Zhang, W.; Pan, W.; Li, C.; Sun, W. Experimental and theoretical investigations on Se(iv) and Se(vi) adsorption to UiO-66-based metal−organic frameworks. *Environ. Sci.: Nano* **2018**, *5*, 1441−1453.
(47) Soltani, R.; Pelalak, R.; Pishnamazi, M.; Marjani, A.; Albadarin, A. B.; Sarkar, S. M.; Shirazian, S. A novel and facile green synthesis method to prepare LDH/MOF nanocomposite for removal of Cd(II) and Pb(II). *Sci. Rep.* **2021**, *11*, No. 1609.
(48) Assaad, N.; Sabeh, G.; Hmadeh, M. Defect Control in Zr-Based Metal−Organic Framework Nanoparticles for Arsenic Removal from Water. *ACS Appl. Nano Mater.* **2020**, *3*, 8997−9008.
(49) Chen, Q.; He, Q.; Lv, M.; Xu, Y.; Yang, H.; Liu, X.; Wei, F. Selective adsorption of cationic dyes by UiO-66-NH2. *Appl. Surf. Sci.* **2015**, *327*, 77−85.
(50) Lin, K.-Y. A.; Liu, Y.-T.; Chen, S.-Y. Adsorption of fluoride to UiO-66-NH2 in water: Stability, kinetic, isotherm and thermodynamic studies. *J. Colloid Interface Sci.* **2016**, *461*, 79−87.
(51) Hasan, Z.; Khan, N. A.; Jhung, S. Adsorptive removal of diclofenac sodium from water with Zr-based metal-organic frameworks. *Chem. Eng. J.* **2016**, *284*, 1406−1413.
(52) Hasan, Z.; Jeon, J.; Jhung, S. H. Adsorptive removal of naproxen and clofibric acid from water using metal-organic frameworks. *J. Hazard. Mater.* **2012**, *209*−*210*, 151−157.
(53) Marx, S.; Kleist, W.; Huang, J.; Maciejewski, M.; Baiker, A. Tuning functional sites and thermal stability of mixed-linker MOFs based on MIL-53(Al). *Dalton Trans.* **2010**, *39*, 3795−3798.
(54) Taddei, M.; Tiana, D.; Casati, N.; van Bokhoven, J. A.; Smit, B.; Ranocchiari, M. Mixed-linker UiO-66: structure-property relationships revealed by a combination of high-resolution powder X-ray diffraction and density functional theory calculations. *Phys. Chem. Chem. Phys.* **2017**, *19*, 1551−1559.
(55) Shearer, G. C.; Chavan, S.; Bordiga, S.; Svelle, S.; Olsbye, U.; Lillerud, K. P. Defect Engineering: Tuning the Porosity and Composition of the Metal-Organic Framework UiO-66 via Modulated Synthesis. *Chem. Mater.* **2016**, *28*, 3749−3761.
(56) Zhao, X.; Wang, Y.; Li, Y.; Xue, W.; Li, J.; Wu, H.; Zhang, Y.; Li, B.; Liu, W.; Gao, Z.; Huang, H. Synergy Effect of Pore Structure and Amount of Carboxyl Site for Effective Removal of Pb2+ in Metal−Organic Frameworks. *J. Chem. Eng. Data* **2019**, *64*, 2728−2735.
(57) Chiban, M.; Soudani, A.; Sinan, F.; Persin, M. Single, binary and multi-component adsorption of some anions and heavy metals on environmentally friendly Carpobrotus edulis plant. *Colloids Surf., B* **2011**, *82*, 267−276.
(58) Fan, X.; Liu, H.; Anang, E.; Ren, D. Effects of Electronegativity and Hydration Energy on the Selective Adsorption of Heavy Metal Ions by Synthetic NaX Zeolite. *Materials* **2021**, *14*, 4066.
(59) Wu, Q.; Dong, S.; Wang, L.; Li, X. Single and Competitive Adsorption Behaviors of Cu2+, Pb2+ and Zn2+ on the Biochar and Magnetic Biochar of Pomelo Peel in Aqueous Solution. *Water* **2021**, *13*, 868.
(60) Wang, K.; Gu, J.; Yin, N. Efficient Removal of Pb(II) and Cd(II) Using NH2-Functionalized Zr-MOFs via Rapid Microwave-Promoted Synthesis. *Ind. Eng. Chem. Res.* **2017**, *56*, 1880−1887.
(61) Howarth, A. J.; Katz, M. J.; Wang, T. C.; Platero-Prats, A. E.; Chapman, K. W.; Hupp, J. T.; Farha, O. K. High Efficiency Adsorption and Removal of Selenate and Selenite from Water Using Metal−Organic Frameworks. *J. Am. Chem. Soc.* **2015**, *137*, 7488−7494.

https://doi.org/10.1021/acsanm.2c02128
ACS Appl. Nano Mater. 2022, 5, 10795−10808

(62) Yang, Q.; Wiersum, A. D.; Llewellyn, P. L.; Guillerm, V.; Serre, C.; Maurin, G. Functionalizing porous zirconium terephthalate UiO-66(Zr) for natural gas upgrading: a computational exploration. *Chem. Commun.* **2011**, *47*, 9603−9605.
(63) Yang, Q.; Vaesen, S.; Ragon, F.; Wiersum, A. D.; Wu, D.; Lago, A.; Devic, T.; Martineau, C.; Taulelle, F.; Llewellyn, P. L.; Jobic, H.; Zhong, C.; Serre, C.; De Weireld, G.; Maurin, G. A Water Stable Metal−Organic Framework with Optimal Features for CO2 Capture. *Angew. Chem., Int. Ed.* **2013**, *52*, 10316−10320.
(64) Pathak, A. K.; Bandyopadhyay, T. Solvation of arsenate anion: combined quantum mechanics and molecular dynamics based investigation. *Mol. Phys.* **2016**, *114*, 2029−2036.
(65) Ali, S.; Zuhra, Z.; Abbas, Y.; Shu, Y.; Ahmad, M.; Wang, Z. Tailoring Defect Density in UiO-66 Frameworks for Enhanced Pb(II) Adsorption. *Langmuir* **2021**, *37*, 13602−13609.
(66) Morcos, G. S.; Ibrahim, A. A.; El-Sayed, M. M. H.; El-Shall, M. S. High performance functionalized UiO metal organic frameworks for the efficient and selective adsorption of Pb (II) ions in concentrated multi-ion systems. *J. Environ. Chem. Eng.* **2021**, *9*, No. 105191.
(67) Liu, J.; Cui, H.; Li, J.; Chen, M. A research on the cadmium ions adsorption of Sulfhydryl- and sulfo-functionalized UIO-66 with silica layer from water. *J. Environ. Chem. Eng.* **2021**, *9*, No. 104621.
(68) Audu, C. O.; Nguyen, H. G. T.; Chang, C.-Y.; Katz, M. J.; Mao, L.; Farha, O. K.; Hupp, J. T.; Nguyen, S. T. The dual capture of AsV and AsIII by UiO-66 and analogues. *Chem. Sci.* **2016**, *7*, 6492−6498.
(69) Wang, C.; Liu, X.; Chen, J. P.; Li, K. Superior removal of arsenic from water with zirconium metal-organic framework UiO-66. *Sci. Rep.* **2015**, *5*, No. 16613.

Recommended by ACS

Rational Construction of Ultrahigh Thermal Stable MOF for Efficient Separation of MTO Products and Natural Gas

Gang-Ding Wang, Zhonghua Zhu, *et al.*
MARCH 09, 2023
ACS MATERIALS LETTERS
READ

γ-Resistant Microporous CAU-1 MOF for Selective Remediation of Thorium

Nitin Gumber, Uttam Kumar Goutam, *et al.*
MARCH 23, 2023
ACS OMEGA
READ

Effects of Nanopore Size on the Adsorption of Sulfamerazine from Aqueous Solution by β-Ketoenamine Covalent Organic Frameworks

Ruiqi Liu, Qin Shuai, *et al.*
DECEMBER 02, 2022
ACS APPLIED NANO MATERIALS
READ

Synergistic Effect of Functionalization and Crystallinity in Nanoporous Organic Frameworks for Effective Removal of Metal Ions from Aqueous Solution

Keyu Li, Pei-Zhou Li, *et al.*
OCTOBER 05, 2022
ACS APPLIED NANO MATERIALS
READ

Get More Suggestions >

https://doi.org/10.1021/acsanm.2c02128
ACS Appl. Nano Mater. 2022, 5, 10795−10808